

1 Seasonal characterization of CDOM for lakes in semi-arid regions of
2 Northeast China using excitation-emission matrices fluorescence and
3 parallel factor analysis (EEM-PARAFAC)

4 Ying Zhao¹, Kaishan Song^{1*}, Zhidan Wen¹, Lin Li², Shuying Zang³, Tiantian Shao¹,

5 Sijia Li¹, Jia Du¹

6 ¹Northeast Institute of Geography and Agroecology, Chinese Academy of Sciences,
7 Changchun, Jilin, 130102, China

8 ²Department of Earth Sciences, Indiana University-Purdue University, Indianapolis,
9 IN, USA

10 ³College of Geographical Science, Harbin Normal University, Harbin, China

11 *corresponding author E-mail: songks@iga.ac.cn; Tel: 86-0431-85542364

12
13 **Abstract.** The seasonal characteristics of fluorescent components in CDOM for lakes
14 in the semi-arid region of Northeast China were examined by excitation-emission
15 matrix (EEM) spectra and parallel factor analysis (PARAFAC). Two humic-like (C1
16 and C2) and the protein-like (C3 and C4) components were identified using
17 PARAFAC. The average fluorescence intensity of the four components differed under
18 seasonal variation from June and August 2013 to February and April 2014.
19 Components 1 and 2 exhibited a strong linear correlation ($R^2 = 0.628$). Significantly
20 positive linear relationships between CDOM absorption coefficients $a(254)$ ($R^2 = 0.72$,
21 0.46 , $p < 0.01$), $a(280)$ ($R^2 = 0.77$, 0.47 , $p < 0.01$), $a(350)$ ($R^2 = 0.76$, 0.78 , $p < 0.01$)
22 and F_{max} for two humic-like components (C1 and C2) were exhibited, respectively. A

23 significant relationship ($R^2 = 0.930$) was found between salinity and DOC. However,
24 almost no obvious correlation was found between salinity and EEM-PARAFAC
25 extracted components except for C3 ($R^2 = 0.469$). Results from this investigation
26 demonstrate that the EEM-PARAFAC technique can be used to evaluate the seasonal
27 dynamics of CDOM fluorescent components for inland waters in the semi-arid
28 regions of Northeast China, and to quantify CDOM components for other waters with
29 similar environmental conditions.

30 **Keywords:** CDOM, fluorescent components, EEMs, PARAFAC, DOC, Salinity

31
32

33 **1 Introduction**

34 Dissolved organic matter (DOM), a heterogeneous mixture of humic acids,
35 proteins and carbohydrates, plays important roles in aquatic ecosystems (Zhang et al.,
36 2010). Chromophoric dissolved organic matter (CDOM), the colored fraction of
37 DOM, absorbs light energy in the ultraviolet (UV) and visible region of the spectrum
38 and inhibits the propagation of UV radiation. CDOM in waters also affects the
39 transport and bio-availability of materials such as trace metals and other pollutants
40 (Song et al., 2013), so it can be used as a proxy of water quality. In natural water
41 bodies, CDOM originates from the degradation of plant materials and other organisms
42 and terrestrially imported substances, which varies in time and space and is controlled
43 by its structure and composition (Stedmon et al., 2003). CDOM is compositionally
44 complex, making it difficult to isolate hydrophobic from hydrophilic acids using XAD
45 ion-exchange resins (Aiken et al., 1992; Spencer et al., 2010). Nonetheless, some

46 optically active components of CDOM can emit fluorescence after absorbing light at
47 certain wavelengths (Zhang et al., 2010) so that the fluorescence spectroscopic
48 techniques can be used to provide detailed information about the source and
49 concentration of CDOM. The traditional fluorescence techniques including
50 fluorescence emission spectrometry and synchronous fluorescence scanning applied
51 to examine CDOM components have the drawback that the output was restricted to a
52 linear scan (Hudson et al., 2007).

53 Recently, excitation-emission matrix fluorescence spectroscopy (EEM) has been
54 applied to identify CDOM components because of its ability to produce synchronous
55 scan spectra in the form of contours (Stedmon et al., 2003; Zhang et al., 2010). The
56 EEM spectroscopy is considered the most effective technique for studying the
57 composition of fluorophores given its high selectivity and sensitivity to CDOM in
58 water columns (Zhang et al., 2010). In recent years, EEM spectroscopy has been
59 widely used to investigate the dynamics of marine, freshwater and ice-water
60 ecosystems as well as snow melting water (Barker et al., 2006, 2009, 2010, 2013;
61 Coble, 2007; Fellman et al., 2010; Guo et al., 2010; Hudson et al., 2007; Stedmon et
62 al., 2007). Moreover, the EEM spectroscopy can also be used to distinguish
63 allochthonous and autochthonous CDOM sources in aquatic environments (Coble et
64 al., 1998; Mayer et al., 1999; Yamashita et al., 2008, 2010; Zhang et al., 2013). Based
65 on the peak positions in EEMs, two main fluorescent components, i.e., humic-like and
66 protein-like substances, have been identified and investigated (DelCastillo et al., 1999;
67 Jaffe' et al., 2004). However, overlapped fluorophores of CDOM EEMs could make

68 this traditional ‘peak-picking’ method unreliable to evaluate CDOM dynamics in
69 aquatic ecosystems (Coble, 1996; Stedmon et al., 2003). Recently, the combined
70 EEMs-PARAFAC (parallel factor analysis) technique has been shown to effectively
71 decompose EEM of CDOM into independent fluorescent components and assess the
72 source of CDOM and relationships with other water quality parameters. A number of
73 investigators have used EEMs-PARAFAC to characterize DOM in freshwater and
74 marine aquatic environments (Broisover et al., 2009; Cory et al., 2005; Guo et al.,
75 2010; Stedmon et al., 2003; Stedmon and Markager, 2005; Yamashita, 2008; Zhang et
76 al., 2010, 2011, 2013). Stedmon et al. (2003) introduced PARAFAC and identified
77 five distinct DOM components for a Danish estuary and its catchment. In coastal
78 environments, Yamashita et al. (2008) reported on seven components using the
79 combined EEMs-PARAFAC technique and assessed the dynamic of individual
80 fluorophores and their relationship with salinity in Ise Bay. Zhang et al. (2011) also
81 found three different components by PARAFAC modeling and analyzed the
82 correlations between the fluorescent components and absorption coefficients of
83 CDOM for Lake Tianmu and its catchment.

84 The Songnen Plain is a fluvial plain with semi-arid climate, in which many fresh
85 and brackish waters are distributed according to its geomorphological characteristics
86 (Song et al., 2013). Dissolved organic carbon (DOC) characteristics of these fresh
87 and brackish waters across the Songnen Plain have been studied by Song et al. (2013);
88 the results indicated that a huge amount of DOC was stored in these waters. In
89 particular, brackish waters would exhibit high average DOC concentrations and

90 significantly contributed the carbon budget to inland waters (Duarte et al., 2008; Song
91 et al., 2013; Tranvik et al., 2009). However, little study has been made on the detailed
92 information of DOC sources for these waters in the Songnen Plain. Therefore, it
93 motivated us to investigate the components in CDOM for both fresh and brackish
94 waters in the semi-arid region. In the present study, the absorption and fluorescence of
95 CDOM were determined for the water samples collected from seven lakes in the
96 western part of Jilin province, which varied at different seasons. The specific
97 objectives of this study are to: 1) characterize CDOM components contained in these
98 lakes using EEMs and their origins through the EEM-PARAFAC method; 2) assess
99 the dynamic of individual fluorescent components of CDOM under seasonal variation;
100 and most importantly 3) link CDOM fluorescence intensities, absorption coefficients,
101 DOC concentrations and salinity to each other, in order to establish proxies for
102 CDOM bioavailability and photoreactivity in waters.

103

104 **2 Materials and Methods**

105 **2.1 Lakes and water sampling**

106 The water bodies investigated in this study were located in the western part of Jilin
107 Province, which belongs to the semi-arid part of the Songnen Plain (Song et al., 2013).
108 Two groups of lakes were investigated, i.e., the Chagan lake group and the Yuelianghu
109 lake group. The Chagan lake group is made up of Lake Chagan (CGL), Xinmiaopao
110 (XMP), Xindianpao (XDP) and Kulipao (KLP). The Yuelianghu lake group mainly
111 includes Lake Yueliang (YLL), Talahong (TLH) and Xinhuangpao (XHP) (Fig. 1).

112 The two groups are about 60 km away from each other, of which each includes both
113 fresh and brackish waters. The primary economic value for these lakes is fisheries,
114 agricultural irrigation and recreation. The average annual precipitation is about 391
115 mm, but the average evaporation is up to 1790 mm, resulting in water scarcity. Due to
116 the area dominated by saline-alkali soil, the rainfall flush and agricultural catchment
117 land use can result in an increase of lake salinities. These seven lakes are endowed
118 with similar geological, hydrological and climatic settings, thus we presume that
119 similar processes may control the CDOM components. In order to characterize the
120 CDOM fluorescent components under seasonal variation using EEMs-PARAFAC, 67
121 water samples were collected from the surface of the seven lakes in 1-liter
122 acid-cleaned plastic bottles during four field campaigns in June and August 2013 as
123 well as in February and April 2014, respectively. These samples were collected during
124 the ice covering period using an ice drilling auger. The under-ice surface water was
125 coming up when a hole was drilled in the ice layer by the auger. The ice shavings
126 were collected in plastic bags and the under-ice surface water was collected in plastic
127 bottles. The collected samples were held on ice and immediately transported to the
128 laboratory in the Changchun City of Jilin province within 3-5 hours. In the laboratory,
129 these samples were filtered within 24 h and then kept at 4 °C until analysis within two
130 days. Latitude and longitude of each sample location were recorded *in situ* using a
131 Trimble Global Positioning System (GPS).

132

133 **Figure 1. Locations of the water sampling sites for 7 lakes in the western part of Jilin**
134 **province, Northeast China. a) Yueliang lake group: YLL, Yueliang Lake; XHP;**

135 **Xinhuangpao; TLH; Talahong; b) Chagan lake group: CGL, Chagan Lake; XDP,**
136 **Xindianpao; XMP, Xinmiaopao; KLP, Kulipao.**

137

138 **2.2 Analytical procedures**

139 To characterize the basic parameters of water quality, salinity was measured through a
140 DDS-307 electrical conductivity (EC) meter in the laboratory. Salinity was expressed
141 in the basis of the UNESCO practical salinity unit. The pH was measured using a
142 PHS-3C pH meter at room temperature (20 ± 2 °C) in the laboratory. Water turbidity
143 was determined using the Shimadzu UV-2600PC UV-Vis dual beam
144 spectrophotometer with matching 3 cm quartz cells at room temperature (20 ± 2 °C)
145 with Milli-Q water as the reference (UV talk letter vol. 10,
146 <https://shimadzu.com.au/uv-talk-letter-volume-10>). To determine DOC concentrations,
147 water samples were filtered through 0.45 µm filters and then measured using a
148 Shimadzu TOC-5000 Analyzer and a 1.2 % Pt on silica catalyst at 680 °C. Potassium
149 hydrogen phthalate was used as a standard. The reproducibility of the analytical
150 procedure was within 2-3 % for the current study (APHA, 1998; Song et al., 2011).

151

152 **2.3 Absorption measurement**

153 In the laboratory, all the samples were filtered at low pressure, first through a
154 pre-combusted Whatman GF/F filter (0.7 µm), and then through a pre-rinsed 25 mm
155 Millipore membrane cellulose filter (0.22 µm) into glass bottles. Absorption spectra of
156 the samples were measured between 200 and 800 nm at 1 nm increments using the
157 Shimadzu UV-2600PC UV-Vis dual beam spectrophotometer with a 1 cm quartz

158 cuvette and Milli-Q water as reference. The absorption coefficient a_{CDOM} was
159 calculated from the measured optical density (OD) of the sample using Eq. (1):

$$160 \quad a_{CDOM}(\lambda) = 2.303 [OD_{(\lambda)} - OD_{(null)}] / \gamma \quad (1)$$

161 where γ is the cuvette path length (0.01 m) and the factor 2.303 converts from base 10
162 to base natural logarithm transformation. Some fine particles possibly remained in the
163 filtered solution (Babin et al., 2003; Bricaud et al., 1995), therefore it was necessary
164 to correct for scattering by fine particles and in this case, $OD_{(null)}$ is the average optical
165 density over 740-750 nm where the absorbance of CDOM can be assumed to be zero.

166 A CDOM absorption spectrum ($a_{CDOM}(\lambda)$) can be expressed as an exponential
167 function (Babin et al., 2003; Bricaud et al., 1995):

$$168 \quad a_{CDOM}(\lambda_i) = a_{CDOM}(\lambda_r) \exp[-S(\lambda_i - \lambda_r)] \quad (2)$$

169 where $a_{CDOM}(\lambda_i)$ is the CDOM absorption at a given wavelength λ_i , $a_{CDOM}(\lambda_r)$ is the
170 absorption estimate at the reference wavelength λ_r (440 nm), and S is the spectral
171 slope of the CDOM absorption. According to Helms et al. (2008), S is calculated by
172 fitting a linear model to the data over a wavelength range of 275 to 295 nm ($S1$) or
173 350 to 400 nm ($S2$). To eliminate the inter-laboratory variability, the slope ratio $S_R =$
174 $S1/S2$ is defined to indicate the molecular weight and photo-bleaching of CDOM
175 (Helms et al., 2008; Zhang et al., 2010).

176

177 **2.4 Three-dimensional fluorescence measurement**

178 The EEMs analysis of CDOM were conducted using a Hitachi F-7000 fluorescence
179 spectrometer (Hitachi High-Technologies, Tokyo, Japan) with a 700-voltage xenon

180 lamp. The scanning ranges were 200–450 nm for excitation, and 250–500 nm for
181 emission. Readings were collected in the ratio mode at 5 nm intervals for excitation,
182 and at 1 nm intervals for emission, using a scanning speed of 2400 nm min⁻¹. The
183 band-passes were 5 nm for both excitation and emission. A Milli-Q water blank of the
184 EEMs was subtracted to eliminate the water Raman scatter peaks (McKnight et al.,
185 2001; Stedmon et al., 2003; Zhang et al., 2010, 2011).

186 The inner-filter effect, which results from reabsorption and excitation of the
187 fluorescence itself, can reduce the fluorescence intensity by 5% (Larsson et al., 2007;
188 McKnight et al., 2001). In order to eliminate the inner-filter effect, the EEMs were
189 corrected for absorbance by multiplying each value in the EEMs with a correction
190 factor based on the assumption that the average path length of absorption of the
191 excitation and emission light is one-half length of the cuvette (McKnight et al., 2001;
192 Zhang et al., 2010). The correction function is expressed as follows:

$$193 \quad F_{corr} = F_{obs} \times 10^{(A_{ex}+A_{em})/2} \quad (3)$$

194

195 where F_{Corr} and F_{obs} are the corrected and uncorrected fluorescence intensities and A_{ex}
196 and A_{em} are the absorbance values at the respective excitation and emission
197 wavelengths.

198 The measured fluorescence intensity is dependent on the concentration of the
199 dissolved fluorophores in water bodies. Finally, the fluorescence intensities of all
200 samples' EEMs were normalized to the area under the Milli-Q water Raman peak
201 (λ_{ex} =350 nm, λ_{em} =371-428 nm) measured daily (Lawaetz and Stedmon, 2009). The

202 contour figures of the EEMs were plotted using the Matlab 10.0 software package
203 (Math Works, Natick Massachusetts, America).

204

205 **2.5 The PARAFAC modeling**

206 PARAFAC, a three-way method, is applied to decompose the CDOM fluorescence
207 into separate fluorescent signals (Andersen and Bro, 2003; Stedmon and Bro, 2008).
208 According to Stedmon and Bro (2008), a similar PARAFAC analysis is carried out in
209 the present study using the DOMFluor toolbox in MATLAB with the “N-way toolbox
210 for MATLAB” (Andersson et al., 2000). Before PARAFAC modeling, the excitation
211 wavelengths from 200 to 220 nm and the emission wavelengths from 250 to 300 nm
212 were deleted because of their poor quality. In order to remove the effect of Rayleigh
213 scatter on PARAFAC modeling, the missing values (NaN-Not a number) were
214 inserted in the regions ($Ex-20 \leq Em \leq Ex+20$ and $2Ex-20 \leq Em \leq 2Ex+20$; unit: nm)
215 which are significantly influenced by the first and second order scattering from the
216 measured spectroscopic data (Hua et al., 2007; Stedmon and Bro, 2008).

217 To determine the appropriate number of PARAFAC components, the split-half
218 validation procedure was executed to verify whether the model was valid by
219 comparing the emission and excitation loadings from each half (Stedmon and Bro,
220 2008). Split-half analysis is the most effective method for implementing the
221 PARAFAC models, in which the EEMs are randomly divided into four groups of
222 equal size, and then analyzed for two half splits (1-2 and 3-4 half) respectively. If the
223 correct number of components is chosen, the excitation and emission loadings from

224 the two groups should show the same shape and size (Bro, 1997, 1999). The
225 fluorescence intensity of every component was represented by F_{max} (Raman unit: nm^{-1})
226 (Stedmon and Markager, 2005).

227

228 **2.6 Statistical analysis**

229 Statistical analysis was conducted using the SPSS 16.0 software package (Statistical
230 Program for Social Sciences). Regression and correlation analysis was used to
231 describe the relationship between CDOM absorption coefficient, DOC concentration,
232 salinity and F_{max} . A model II-ANOVA was performed to determine seasonal
233 variability is higher than between-lake variability. The difference is considered to be
234 statistically significant when p -values are less than or equal to 0.05.

235

236 **3 Results and discussion**

237 **3.1 Water quality conditions**

238 The water quality parameters, i.e., pH, salinity, turbidity for the 67 water samples
239 collected from June 2013 to April 2014 in the western part of Jilin province are
240 displayed in Table 1. When the set of samples from various field trips was pooled
241 together, the waters had high pH values and high salt contents. The highest salinity
242 was present when the lakes were frozen in February 2014, whereas relatively constant
243 values (around 0.40) were exhibited in the other three seasons. Also the water bodies
244 were highly turbid. The highest turbidity was present in June 2013, and then reduced
245 in August 2013, and the lowest value was recorded in February 2014. Compared with

246 February 2014, the turbidity had almost no change in April 2014 (Table 1).

247

248 **Table 1. Mean value of water quality parameters from June 2013 to April 2014.**

249

250 **3.2 EEMs characterization of CDOM**

251 Based on the EEMs ‘peak picking’ technique, the key fluorescence peaks can be
252 observed in 67 water samples: two humic-like and two protein-like substances (Coble,
253 1996; Stedmon et al., 2003). The humic-like components are the mixture of aromatic
254 and aliphatic compounds-humic-like acids from terrestrial substances, and aquatic
255 humic-like substances of phytoplankton origin. With respect to the protein-like
256 components (i.e., tyrosine-like and tryptophan-like substance), they mainly consist of
257 dissolved amino acids. As an example, Fig. S1 displays the EEMs of samples from
258 lake Xindianpao at different seasons. The peaks comprise two humic-like
259 fluorescence peaks: one in the ultraviolet range (Ex/Em = 220-240/410-430 nm) and
260 the other in the visible range (Ex/Em = 300-340/410-450 nm) and the protein-like
261 fluorescence peaks: tyrosine-like (Ex/Em = 210-230, 270-280/310-330 nm) and
262 tryptophan-like (Ex/Em = 220-230, 280-300/350-370 nm).

263

264 In our study, four separate fluorescent components (Fig. 2a-d) and the
265 excitation and emission loadings (e-h) of the four components identified by
266 EEM-PARAFAC are summarized in Fig. 2 and Table 2. The first fluorescent
267 component (C1) was a biological degradation humic-like component comparable to

268 humic-like peaks (M and N) in marine and in phytoplankton degradation experiments
269 for inland waters (Coble, 1996; Zhang et al., 2009). Component 2 was consistent with
270 the humic-like peaks (A and C) defined by Coble (1996). Component 3 resembles the
271 tryptophan-like (T) component as found by Baker et al. (2004) and Hudson et al.
272 (2007). For component 4, it is likely related to tyrosine-like component (B) (Hudson
273 et al., 2007). Components 3 and 4 represent autochthonous semi-labile CDOM
274 associated with bacteria activity and phytoplankton degradation (Borisover et al.,
275 2009; Stedmon et al., 2003). Particularly, there was a shoulder at the excitation
276 wavelength 310-330 nm in component 3 and 330-340 nm in component 4, which may
277 be due to the residual Raman peaks in some water samples (Fig. 2c-d). In this study,
278 not all of the four components were present in all of the samples.

279

280 **Figure 2. The PARAFAC modeling output shows the contour plots of the four PARAFAC**
281 **fluorescent components (a-d) and excitation (black) and emission (red) loadings (e-h) of each**
282 **component. Fluorescence is in Raman units: nm⁻¹.**

283

284 **Table 2. Positions of the fluorescence maximum peaks of the four components identified by**
285 **PARAFAC modeling in the present study compared with those previously identified.**
286 **Secondary excitation maxim is given in brackets.**

287

288 **3.3 Temporal distribution of PARAFAC components**

289 These fresh and brackish water in Jilin province in northeast China are endowed with
290 similar geological, hydrological and climatic settings, thus it is presumed that similar
291 processes may control the CDOM components. When a model II-ANOVA using

292 season and lake as random effect factors was performed, it shows that the seasonal
293 variability ($F > F_{crit}$, $p < 0.05$) is higher than between-lake variability. Therefore, the
294 water samples from different lakes for every season were pooled together in order to
295 study the seasonal variation of the fluorescent components. As shown in Fig. 3a, the
296 average fluorescence intensity of the four components had seasonal variation. When
297 all the water samples at different seasons were pooled together, the average value of
298 total fluorescence intensity was $2.05 \pm 0.93 \text{ nm}^{-1}$, corresponding to the intensities of
299 0.71 ± 0.32 (C1), 0.33 ± 0.11 (C2), 0.50 ± 0.24 (C3), and 0.51 ± 0.26 (C4) nm^{-1} for
300 different components. These results can demonstrate that the fluorescence intensity
301 was dominated by C1, implying most of the CDOM for the seven inland lakes
302 originated from the degradation of phytoplankton and microorganisms. The
303 protein-like components (C3 and C4), related to bioavailability and microbial activity
304 of CDOM, had almost the same magnitude. At all four seasons, the fluorescent
305 component C2, which was terrestrially imported to water bodies, contributed less to
306 total fluorescence than the other three. The total fluorescence intensity differed under
307 seasonal variation, varying from $2.54 \pm 0.68 \text{ nm}^{-1}$ in June to $1.93 \pm 0.70 \text{ nm}^{-1}$ in
308 August 2013, and then increased to $2.34 \pm 0.92 \text{ nm}^{-1}$ in February and reduced to the
309 lowest $1.57 \pm 0.55 \text{ nm}^{-1}$ in April 2014 (Fig. 3c). The intensities of four fluorescent
310 components (i.e., 0.75 ± 0.17 (C1), 0.32 ± 0.06 (C2), 0.69 ± 0.24 (C3), and $0.77 \pm$
311 0.20 (C4) nm^{-1}) (Fig. 3d) from the samples collected in June 2013 exhibited similar
312 trends to that for the pooled data set. These values were higher than the seasonal
313 average except C2 ($0.32 \pm 0.06 \text{ nm}^{-1}$). This can be explained by enhanced activities

314 from plant degradation and microbial activities, but less terrestrial substances were
315 imported to the water bodies in June and therefore the fluorescence intensity of C2
316 was lower than the seasonal average. Compared to the fluorescence intensity in June,
317 the three fluorescence intensities (0.65 ± 0.14 (C1), 0.33 ± 0.16 (C3), 0.52 ± 0.36 (C4)
318 nm^{-1}) from the samples collected in August 2013 were reduced, but an increased value
319 was recorded for C2 ($0.42 \pm 0.05 \text{ nm}^{-1}$) (Fig. 3d). Especially, the fluorescence
320 intensities of two protein-like components showed an obvious difference. This can be
321 attributed to substantially increased precipitation up to 180 mm in July from June to
322 August 2013 (Fig. 3b) so that floods occurred when rainfall continued to increase in
323 August. Gradually, DOM contained in terrestrial CDOM was flushed by rainfall to the
324 lakes so that the C2 ($0.42 \pm 0.05 \text{ nm}^{-1}$) fluorescence intensity became higher. In
325 accordance with Cheng et al. 2010, the rainwater CDOM for this study was largely
326 characterized by protein-like components (Cheng et al., 2010). The fluorescence
327 intensity of the rainwater CDOM was very weak, and also the rainwater CDOM
328 contained much lower humic-like concentration (Fig. S2b). The intensities of the
329 other three components decreased because of dilution resulting from heavy rain and
330 relatively weak microbial decomposition of plants.

331 The highest C1 ($1.02 \pm 0.38 \text{ nm}^{-1}$) presented in February 2014, and the C2 (0.39
332 $\pm 0.12 \text{ nm}^{-1}$) intensity remained almost the same as that in August 2013. However, the
333 protein-like components indicated that the C3 ($0.57 \pm 0.25 \text{ nm}^{-1}$) intensity was higher
334 than the C4 ($0.35 \pm 0.17 \text{ nm}^{-1}$) intensity, which was opposite to the results from other
335 months (Fig. 3d). In cold winter, the surface waters formed a thick layer of ice

336 covering the lake waters. Because the ice cover reduced light penetration and
337 restricted gas exchange between the underlying water and atmosphere, vigorous
338 biological activity in the lakes would be reduced at low temperature and low light
339 level (Thomas K., 1983; Uusikiv et al., 2010; Wharton, et al., 1993). Although the
340 biological activity was very weak, there could still be a bit of production of C1 and
341 C3 in lake water. Also, dissolved materials were left in the underlying surface waters
342 and little terrestrial matter was imported to the lakes once covered by ice (Stedmon et
343 al., 2007). Therefore, the C1 and C3 in the water of the lakes beneath the ice layers
344 would be produced and accumulated simultaneously, whereas, the C2 remained the
345 same. Obviously, the fluorescence intensity of component 1 reached the highest value
346 for the winter samples. As shown in Fig. S2a, another striking feature for the winter
347 samples was that the fluorescence of CDOM in the ice was dominated by the
348 tyrosine-like C4 component, which is consistent with the findings of Barker et al.
349 (2009, 2013) and Stedmon et al. (2007). It showed that the C4 component was left in
350 the ice-cover when the lakes were frozen. Therefore, it is not surprising that the
351 intensity of component C4 for water beneath ice layers was reduced and the
352 concentrated C3 showed a much higher fluorescence intensity. In April 2014, the
353 intensities of four fluorescent components (0.47 ± 0.17 (C1), 0.25 ± 0.08 (C2), $0.40 \pm$
354 0.16 (C3), and 0.45 ± 0.13 (C4) nm^{-1}) (Fig. 3d) exhibited similar seasonal trends
355 though these values were much lower than the average. Our interpretation is that the
356 ice CDOM was characterized by tyrosine-like component (C4) (Fig. S2a), and the
357 fluorescence intensity of C4 contributed by the ice-melt water was very weak.

358 However, the underlying lake CDOM included both humic-like (C1 and C2) and
359 protein-like (C3 or C4) components. When the ice in the lakes melted into water with
360 warming weather and biological degradation and human activity was weak, the lake
361 CDOM was diluted by the ice-melted water and the fluorescence intensity would
362 reach to the lowest value in early spring.

363

364 **Figure 3. a) Seasonal average of F_{max} for EEM-PARAFAC components (C1, C2, C3 and C4)**
365 **for lakes in the western part of Jilin province; b) Monthly variation of rainfall for the lakes**
366 **in western part of Jilin province from April 2013 to February 2014; c) Seasonal variation of**
367 **the total fluorescence intensity at different seasons; d) Seasonal variation of the four**
368 **EEM-PARAFAC components at different seasons. The error bars represent one standard**
369 **deviation.**

370

371 **3.4 CDOM versus EEM-PARAFAC extracted components**

372 The concentration of DOC, CDOM absorption coefficients and the slope ratio S_R are
373 shown in Table 3. The DOC concentrations ranged from 835.83 to 7345.83 $\mu\text{mol L}^{-1}$
374 with an average value of $3133.05 \pm 1504.14 \mu\text{mol L}^{-1}$ during the period from June
375 2013 to April 2014, demonstrating a seasonal dynamics that can be attributed to
376 hydrological, climatic and landscape variations (Song et al., 2013). The highest
377 average DOC concentration ($4587.03 \pm 1666.83 \mu\text{mol L}^{-1}$) was present in February
378 2014 (ice-covered period); whereas, relatively constant values of approximate 2500
379 $\mu\text{mol L}^{-1}$ were observed in the ice-free season. The relative high DOC concentration in
380 ice-free season was caused by evapo-condensed effect due to the prolonged sunshine
381 duration for the lakes in the Songnen Plain. With respect to the higher DOC

382 concentration in winter, it can be attributed to the accumulated DOC left in the liquid
383 phase when ice formation took place, resulting in the higher DOC concentration in the
384 underlying water (unpublished material). Generally, the absorption coefficient $a(350)$
385 is used as a proxy for characterizing CDOM concentration (Guo et al., 2010; Zhang et
386 al., 2011), $a(280)$ is related to DOC biodegradation (McDowell et al., 2006), and
387 $a(254)$ can be used to characterize the optical properties of DOC aromaticity (Jaffe' et
388 al., 2004; Weishaar et al., 2003). The highest averaged CDOM absorption coefficients
389 $a(350)$, $a(280)$, $a(254)$ were also present in February 2014, corresponding to the
390 highest DOC concentration. The S_R values of the two wavelength ranges (275-295 nm
391 over 350-400 nm) were used to represent DOM molecular weight (Helms et al., 2008).
392 The lowest mean of S_R was present in August 2013 suggesting the relatively weak
393 microbial decomposition of plants and lots of terrestrially imported substances
394 through rainwash resulted in the higher average molecular weight of DOC.

395

396 **Table 3. Mean values of DOC concentration and CDOM absorption coefficients groups at**
397 **different seasons. S_R : the slope ratio of $S_{275-295\text{nm}}$: $S_{350-400\text{nm}}$.**

398

399 When the whole data set ($N = 67$) was pooled together, there were significantly
400 positive linear relationships between $a(254)$, $a(280)$, $a(350)$ and F_{max} for two
401 humic-like components (C1 and C2), respectively, but mostly such correlations were
402 not observed for the protein-like components (Fig. 4a and b, Table 3). These results
403 were in accordance with previous investigations (Zhang et al., 2010, 2011).
404 Components 1 and 2 were strongly linearly correlated with each other ($R^2 = 0.628$)

405 (Fig. 4c), indicating that the concentrations of the two humic-like components were
406 controlled by common sources (Baker and Spencer, 2004). There was a weak
407 relationship ($R^2 = 0.051$) between the protein-like components (C3 and C4) possibly
408 because of a complex origin of CDOM such as rainfall in summer, ice in winter and
409 organic pollutants derived from domestic, agricultural and industrial sewerage, which
410 represent the complex origins of CDOM. However, there was almost no correlation
411 between the humic-like and protein-like components. The linkage of a fluorescence
412 signal to DOC was very complicated because of the seasonal impacts, i.e., increased
413 rainfall, algal blooms and ice-cover, which affect the DOC concentration. Due to both
414 steady and labile CDOM fluorescent components in DOC, the fluorescent signal
415 would change with the ratio of fluorescent and non-fluorescent CDOM components
416 (Henderson et al., 2009). A weak relationship ($R^2 = 0.411$) (Fig. 4d) was found
417 between DOC and component 3 likely from the decay of plants through microbial
418 activity or the pollution from human and animal wastes.

419 Different from the findings by Yamashita et al. (2008) for ocean water, this study
420 did not find obvious correlation between salinity and EEM-PARAFAC extracted
421 components with the exception of C3 ($R^2 = 0.469$) (Table 4 and Fig. 4f). The most
422 important finding for the water samples collected at different seasons from the
423 Songnen Plain is a significant relationship ($R^2 = 0.930$) between salinity and DOC
424 (Fig. 4e). This is because DOC is evapo-condensed from spring to autumn and
425 freeze-accumulated in winter in the semi-arid region. A prolonged sunshine duration
426 can result in an evapo-condensed DOC concentration in ice-free season. On the other

427 hand, the DOC is accumulated when the lakes freeze in winter leaving DOC in the
428 liquid phase.

429

430 **Table 4. Correlation coefficients (R) and significance levels (p) of the linear relationships**
431 **between CDOM absorption, DOC, salinity and fluorescent components.**

432

433 **Figure 4. Relationships between CDOM absorption coefficient a(350) with a) $F_{max}(C1)$, b)**
434 **with $F_{max}(C2)$, c) peak $F_{max}(C1)$ versus $F_{max}(C2)$, d) peak $F_{max}(C3)$ versus DOC, e) Salinity**
435 **versus DOC, f) Salinity versus $F_{max}(C3)$.**

436

437 **4 Conclusions**

438 A model II-ANOVA using season and lake as random effect factors shows that the
439 seasonal variability ($F > F_{crit}$, $p < 0.05$) is higher than between-lake variability. In this
440 study, the application of EEM-PARAFAC to characterize four fluorescent
441 components under seasonal variation in CDOM was presented with 67 water samples
442 collected from June 2013 to April 2014 in the semi-arid region of the Songnen Plain.
443 Two humic-like and the protein-like components were identified using the PARAFAC
444 modeling. The average fluorescence intensity of the four components differed under
445 seasonal variation from June 2013 to April 2014. The highest C1 1.02 nm^{-1} was
446 presented in February 2014 probably due to the condensed CDOM caused by ice
447 formation in winter. Especially in summer when quantities of rainfall take place and
448 in winter when water is frozen, the fluorescence intensity is dominated by
449 tyrosine-like components in rain and ice-melt water. Component 1 and 2 exhibited a
450 strong linear correlation ($R^2 = 0.628$). There were significantly positive linear

451 relationships between F_{max} and CDOM absorption coefficient $a(254)$ ($R^2 = 0.72$, 0.46 ,
452 $p < 0.01$), $a(280)$ ($R^2 = 0.77$, 0.47 , $p < 0.01$), $a(350)$ ($R^2 = 0.76$, 0.78 , $p < 0.01$) for two
453 humic-like components (C1 and C2), respectively. A weak relationship ($R^2 = 0.411$)
454 was found between DOC and component 3 from the decay of plants through
455 microbial activity or the pollution from human and animal wastes. However, almost
456 no obvious correlation was found between salinity and EEM-PARAFAC extracted
457 components except C3 ($R^2 = 0.469$), though the correlation was not as strong as with
458 DOC concentration. Most importantly, a significant relationship ($R^2 = 0.930$) was
459 found between salinity and DOC. In order to understand the biogeochemical effects
460 on the aquatic ecosystem, further study should be required to identify CDOM source
461 and assess physical/chemical, bioavailable and photoreactive transformation in
462 various lakes with larger saline gradients in the semi-arid region, Northeast China.

463

464 **Acknowledgements**

465 The research was jointly supported by the “One Hundred Talents” program from
466 Chinese Academy of Sciences and the National Natural Science Foundation of China
467 (No. 41471290). The authors thank Zhi Ding, Ying Guan, Lei Liu and Ming Wang for
468 their persistent assistance with both field sampling and laboratory analysis.

469

470 **References**

471 APHA/AWWA/WE F.: Standard Methods for the Examination of Water and

472 Wastewater, Washington, DC: American Public Health Association, 1998.

473 Aiken, G. R., McKnight, D. M., Thorn, K. A., and Thurman, E. M.: Isolation of
474 hydrophobic organic-acids from water using nonionic macro porous resins, *Org.*
475 *Geochem.*, 18, 567-573, 1992.

476 Andersen, C. M., and Bro, R.: Practical aspects of PARAFAC modeling of
477 fluorescence excitation-emission data, *J. Chemom.*, 17, 200-215, 2003.

478 Andersso, C. A., and Bro. R.: The N-way Toolbox for MATLAB, *Chemom. Intell.*
479 *Lab. Syst.*, 52, 1-4, 2000.

480 Babin, M., Stramski, D., Ferrari, G. M., Claustre, H., Bricaud, A., Obolensky, G.,
481 and Hoepffner, N.: Variations in the light absorption coefficients of
482 phytoplankton, nonalgal particles, and dissolved organic matter in coastal waters
483 around Europe, *J. Geophys. Res.*, 108, 3211-3230, 2003.

484 Baker, A., Ward, D., Lieten, Shakti H., Periera, R., Simpson, Ellie C., and Slater, M.:
485 Measurement of protein-like fluorescence in river and waste water using a
486 handheld spectrophotometer, *Water Res.*, 38, 2934-2938, 2004.

487 Baker, A., and Spencer, R. G. M.: Characterization of dissolved organic matter from
488 source to sea using fluorescence and absorbance spectroscopy, *Sci. Total*
489 *Environ.*, 333, 217-232, 2004.

490 Barker, J. D., Dubnick, A., Lyons, W. B., and Chin, Y. P.: Changes in Dissolved
491 Organic Matter (DOM) Fluorescence in Proglacial Antarctic Streams, *Arct.*
492 *Antarct. Alp. Res.*, 45, 305-317, 2013.

493 Barker, J. D., Sharp, M. J., Fitzsimons, S. J., and Turner, R. J.: Abundance and
494 dynamics of dissolved organic carbon in glacier systems, *Arct. Antarct. Alp. Res.*,
495 38, 163–172, 2006.

496 Barker, J. D., Sharp, M. J., and Turner, R. J.: Using synchronous fluorescence
497 spectroscopy and principal components analysis to monitor dissolved organic
498 matter dynamics in a glacier system, *Hydrol. Processes*, 23, 1487–1500, 2009.

499 Barker, J. D., Klassen, J. L., Sharp, M. J., Fitzsimons, S. J., and Turner, R. J.:
500 Detecting biogeochemical activity in basal ice using fluorescence spectroscopy,
501 *Ann. Glaciol.*, 51, 47–55, 2010.

502 Borisover, M., Laor, Y., Parparov, A., Bukhanovsky, N., and Lado, M.: Spatial and
503 seasonal patterns of fluorescent organic matter in Lake Kinneret (Sea of Galilee)
504 and its catchment basin, *Water Res.*, 43, 3104-3116, 2009.

505 Bricaud, A., Babin, M., Morel, A., and Claustre, H.: Variability in the
506 chlorophyll-specific absorption coefficients of natural phytoplankton: Analysis
507 and parameterization, *J. Geophys. Res.*, 100, 13321–13332, 1995.

508 Bro, R.: PARAFAC tutorial and applications, *Chemom. Intell. Lab. Syst.*, 38, 149-171,
509 1997.

510 Bro, R.: Exploratory study of sugar production using fluorescence spectroscopy and
511 multi-way analysis, *Chemom. Intell. Lab. Syst.*, 46,133-147, 1999.

512 Cheng, Y. Y., Guo, W. D., Long, A. M., and Chen, S. Y.: Study on optical
513 characteristic of chromophoric dissolved organic matter in rainwater by

514 fluorescence excitation-emission matrix and absorbance spectroscopy (Article in
515 Chinese), *Spectrosc. Spect. Anal.*, 30, 2413-2416, 2010.

516 Coble, P. G.: Characterization of marine and terrestrial DOM in seawater using
517 excitation-emission matrix spectroscopy, *Mar. Chem.*, 51, 325–346, 1996.

518 Coble, P. G.: Marine optical biogeochemistry: the chemistry of ocean color, *Chem.*
519 *Rev.*, 107, 402-418, 2007.

520 Coble, P. G., Del Castillo, C. E., and Avril, B.: Distribution and optical of CDOM in
521 the Arabian Sea during the 1995 Southwest Monsoon, *Deep-Sea Res. part II*, 45,
522 2195–2223, 1998.

523 Cory, R. M., and McKnight, D. M.: Fluorescence spectroscopy reveals ubiquitous
524 presence of oxidized and reduced quinines in dissolved organic matter, *Environ.*
525 *Sci. Technol.*, 39, 8142-8149, 2005.

526 DelCastillo, C. E., Coble, P. G., Morell, J. M., Lopez, J. M., and Corredor, J. E.:
527 Analysis of the optical properties of the Orinoco River plume by absorption and
528 fluorescence spectroscopy, *Mar. Chem.*, 66, 35–51, 1999.

529 Duarte, C. M., Montes, C., Cole, J. J., Striegl, R. G., Melackand, J., and Downing, J.
530 A.: CO₂ emissions from saline lakes: A global estimate of a surprisingly large flux,
531 *J. Geophys. Res. Biogeosci.*, 113, G04041, 2008.

532 Fellman, J. B., Hood, E., and Spencer, R. G. M.: Fluorescence spectroscopy opens
533 new windows into dissolved organic matter dynamics in freshwater ecosystems:
534 A review, *Limnol. Oceanogr.*, 55, 2452-2462, 2010.

535 Guo, W. D., Xu, J., Wang, J. P., Wen, Y. G., Zhou, J. F., and Yan, Y. C.:
536 Characterization of dissolved organic matter in urban sewage using excitation
537 emission matrix fluorescence spectroscopy and parallel factor analysis, *J.*
538 *Environ. Sci.*, 22, 1728-1734, 2010.

539 Henderson, R. K., Baker, A., Murphy, K. R., Hambly, A., Stuetz, R. M., and Khan, S.
540 J.: Fluorescence as a potential monitoring tool for recycled water system: A
541 review, *Water Res.*, 43, 863-881, 2009.

542 Helms, J. R., Stubbins, A., Ritchie, J. D., Minor, E. C., Kieber, D. J., and Mopper, K.:
543 Absorption spectral slopes and slope ratios as indicators of molecular weight,
544 source, and photo bleaching of chromophoric dissolved organic matter, *Limnol.*
545 *Oceanogr.*, 53, 955–969, 2008.

546 Hua, B., Dolan, F., Mcghee, C., Clevenger, ThomasE., and Deng, B. L.: Water-source
547 characterization and classification with fluorescence EEM spectroscopy:
548 PARAFAC analysis, *Int. J. Environ. Anal. Chem.*, 87, 135-147, 2007.

549 Hudson, N., Baker, A., and Reynolds, D.: Fluorescence analysis of dissolved organic
550 matter in natural, waste and polluted waters – a review, *River Res. Appl.*, 23,
551 631–649, 2007.

552 Jaffe', R., Boyer, J. N., Lu, X., Maie, N., Yang, C., Scully, N. M., and Mock, S.:
553 Source characterization of dissolved organic matter in subtropical
554 mangrove-dominated estuary by fluorescence analysis, *Mar. Chem.*, 84, 195–210,
555 2004.

556 Larsson, T., Wedborg, M., and Turner, D.: Correction of inner-filter effect in
557 fluorescence excitation-emission matrix spectrometry using Raman scatter, *Anal.*
558 *Chim. Acta.*, 583, 357-363, 2007.

559 Lawaetz, A. J., and Stedmon, C. A.: Fluorescence Intensity Calibration Using the
560 Raman Scatter Peak of Water, *Appl. Spectrosc.*, 63, 936-940, 2009.

561 Mayer, L. M., Schick, L. L., and Loder, T. C.: Dissolved protein fluorescence in two
562 Maine estuaries, *Mar. Chem.*, 64, 171–179, 1999.

563 McDowell, W. H., Zsolnay, A., Aikenhead-Peterson, J. A., Gregorich, E. G., Jones, D.
564 L., Joërdmann, D., Kalbitz, K., Marschner, B., and Schwesig, D.: A
565 comparison of methods to determine the biodegradable dissolved organic
566 carbon from different terrestrial sources, *Soil Biol. Biochem.*, 38, 1933–1942,
567 2006.

568 Mcknight, D. M., Boyer, E. W., Westerhoff, P. K., Doran, P. T., Kulbe, T., and
569 Andersen, D. T.: Spectrofluorometric characterization of dissolved organic
570 matter for indication of precursor organic material and aromaticity, *Limnol.*
571 *Oceanogr.*, 46, 38–48, 2001.

572 Song, C. C., Wang, L. L., Guo, Y. D., Song, Y. Y., Yang, G. S., and Li, Y. C.: Impacts
573 of natural wetland degradation on dissolved carbon dynamics in the Sanjiang
574 Plain, Northeastern China, *J. Hydrol.*, 398, 26-32, 2011.

575 Song, K. S., Zang, S. Y., Zhao, Y., Du, J., Lin, L., Zhang, N. N., Wang, X. D., Shao, T.
576 T., Guan, Y., and Liu, L.: Spatiotemporal characterization of dissolved carbon

577 for inland waters in semi-humid/semiarid region, China, *Hydrol. Earth Syst.*
578 *Sci.*, 17, 4269-4281, 2013.

579 Spencer, R. G. M., Hernes, P. J., Ruf, R., Baker, A., Dyda, R. Y., Stubbins, A., and
580 Six, J.: Temporal controls on dissolved organic matter and lignin
581 biogeochemistry in a pristine tropical river, *J. Geophys. Res. Biogeosci.*, 115,
582 G03013, 2010.

583 Stedmon, C. A., and Bro, R.: Characterizing dissolved organic matter fluorescence
584 with parallel factor analysis: a tutorial, *Limnol. Oceanogr. Methods*, 6, 572-579,
585 2008.

586 Stedmon, C. A., and Markager, S.: Tracing the production and degradation of
587 autochthonous fractions of dissolved organic matter by fluorescence analysis,
588 *Limnol. Oceanogr.*, 50, 1415-1426, 2005.

589 Stedmon, C. A., Markager, S., and Bro, R.: Tracing dissolved organic matter in
590 aquatic environments using a new approach to fluorescence spectroscopy, *Mar.*
591 *Chem.*, 82, 239-254, 2003.

592 Stedmon, C. A., Thomas, D. N., Granskog, M., Kaartokallio, H., Papadimitriou, S.,
593 and Kuosa, H.: Characteristics of dissolved organic matter in Baltic coastal sea
594 ice: allochthonous or autochthonous origins? *Environ. Sci. Technol.*, 41,
595 7273–7279, 2007.

596 Thomas K. B.: Under Landfast ice, *Arctic*, 36, 328-340, 1983.

597 Tranvik, L. J., Downing, J. A., Cotner, J. B., Loiselle, S. A., Striegl, R. G., Ballatore, T.

598 J., Dillon, P., Finlay, K., Fortino, K., Knoll, L. B., Kortelainen, P. L., Kutser, T.,
599 Larsen, S., Laurion, I., Leech, D. M., McCallister, S. L., McKnight, D. M.,
600 Melack, J. M., Overholt, E., Porter, J. A., Prairie, Y., Renwick, W. H., Roland, F.,
601 Sherman, B. S., Schindler, D. W., Sobek, S., Tremblay, A., Vanni, M. J.,
602 Verschoor, A. M., Wachenfeldt, E. V., and Weyhenmeyer, G. A.: Lakes and
603 reservoirs as regulators of carbon cycling and climate, *Limnol. Oceanogr.*, 54,
604 2298–2314, 2009.

605 Uusikiv, J., Vahatal, A.V., Granskog, M.A., Sommaruga, R., 2010. Contribution of
606 mycosporine-like amino acids and colored dissolved and particulate matter to
607 sea ice optical properties and ultraviolet attenuation, *Limnol. Oceanogr.*, 55(2),
608 703–713.

609 UV talk letter vol. 10, 2013. <https://shimadzu.com.au/uv-talk-letter-volume-10>

610 Weishaar, J. L., Aiken, G. R., Bergamaschi, B. A., Farm, M. S., Fujii, R., and Mopper,
611 K.: Evaluation of specific ultraviolet absorbance as an indicator of the chemical
612 composition and reactivity of dissolved organic carbon, *Environ. Sci. Technol.*,
613 37, 4702–4708, 2003.

614 Wharton, R. A., Jr., McKay, C. P., Clow, G. D., and Andersen, D. T.: Perennial ice
615 covers and their influence on Antarctic lake ecosystems, *Antarct. Res. Ser.*, 59,
616 53–70, 1993.

617 Yamashita, Y.: Assessing the dynamics of dissolved organic matter (DOM) in coastal
618 environments by excitation emission matrix fluorescence and parallel factor
619 analysis (EEM-PARAFAC), *Limnol. Oceanogr.*, 53, 1900-1908, 2008.

620 Yamashita, Y., Cory, R. M., Nishioka, J., Kuma, K., Tanoue, E., and Jaffe', R.,:
621 Fluorescence characteristics of dissolved organic matter in the deep waters of the
622 Okhotsk Sea and the northwestern North Pacific Ocean, *Deep Sea Res. Part II*,
623 57, 1478–1485, 2010.

624 Zhang, Y. L., Liu, X. H., Osburn, C. L., Wang, M. Z., Qin, B. Q., and Zhou, Y. Q.:
625 Photo bleaching response of different Source of Chromophoric Dissolved
626 Organic Matter Exposed to Natural Solar Radiation Using Absorption and
627 Excitation-Emission Matrix Spectra, *Plos one*, 8, e77515, 2013.

628 Zhang, Y. L., Yin, Y., Feng, L. Q., Zhu, G. W., Shi, Z. Q., Liu, X. H., and Zhang, Y. Z.:
629 Characterizing chromophoric dissolved organic matter in Lake Tianmuhu and its
630 catchment basin using excitation-emission matrix fluorescence and parallel
631 factor analysis, *Water Res.*, 45, 5110-5122, 2011.

632 Zhang, Y. L., Zhang, E. L., Yin, Y., VanDijk, M. A., Feng, L. Q., Shi, Z. Q., Liu, M. L.,
633 and Qin, B. Q.: Characteristics and sources of chromophoric dissolved organic
634 matter in lakes of the Yungui Plateau, China, differing in trophic state and
635 altitude, *Limnol. Oceanogr.*, 55, 2645-2659, 2010.

636 Zhang, Y. L., VanDijk, M. A., Liu, M. L., Zhu, G. W., and Qin, B. Q.: The
637 contribution of phytoplankton degradation to chromophoric dissolved organic
638 matter (CDOM) in eutrophic shallow lakes: Field and experimental evidence.
639 *Water Res.*, 43, 4685–4697, 2009.

640

641

642 Table 1. Mean value of water quality parameters from June 2013 to April 2014. Turb
643 denotes water turbidity; N denotes sampling numbers.

644

Sampling season	pH	Salinity	Turb (NTU)	N
Jun.2013	8.54	0.40	166.20±108.73	15
Aug.2013	8.63	0.37	63.13±31.21	13
Feb.2014	8.35	0.70	21.33±15.87	17
Apr.2014	8.67	0.43	22.24±16.42	22
All	8.55	0.48	62.18±79.07	67

645

646

647

648

649

650

651

652

653

654

655

656

657

658

659

660

661

662

663

664

665

666

667 Table 2. Positions of the fluorescence maximum peaks of the four components
 668 identified by PARAFAC modeling in the present study compared with those
 669 previously identified. Secondary excitation maxima is given in brackets.

670

Component No	Ex _{max} (nm)	Em _{max} (nm)	Description and source	Components (Coble) and (Zhang)	Components (Stedmon and Markager)
C1	230 (300)	425	Marine humic-like (phytoplankton degradation)	M	6
C2	255 (350)	460	Terrstrial humic-like	A and C	1 and 4
C3	225 (290)	360	Autochthonous tryptophan-like	T	
C4	220 (275)	320	Autochthonous tyrosine-like	B	8

671 Fluorescence peaks were named as Components (Coble) and (Zhang) by Coble et al. (1996, 1998) and Zhang et al.
 672 (2010, 2011), while as Components (Stedmon and Markager) by Stedmon and Markager (2005).

673

674

675

676

677

678

679

680

681

682

683

684

685

686

687

688

689

690 Table 3. Mean values of DOC concentration and CDOM absorption coefficients
 691 groups at different seasons. S_R : the slope ratio of $S_{275-295nm} : S_{350-400nm}$.

Sampling season	a(254) m ⁻¹	a(280) m ⁻¹	a(350) m ⁻¹	S_R	DOC μmol L ⁻¹	N
Jun.2013	38.39±9.23	25.98±6.38	5.73±1.68	1.29±0.16	2653.08±1222.14	15
Aug.2013	29.71±4.73	19.36±2.91	5.82±0.81	0.96±0.22	2735.99±1231.61	13
Feb.2014	52.88±18.13	34.62±11.54	6.36±2.17	1.18±0.11	4587.03±1666.83	17
Apr.2014	34.43±11.38	22.45±7.36	4.17±1.49	1.32±0.13	2571.38±909.47	22
All	39.08±14.73	25.73±9.58	5.40±1.84	1.21±0.20	3133.05±1504.14	67

693
 694
 695
 696
 697
 698
 699
 700
 701
 702
 703
 704
 705
 706
 707
 708
 709
 710
 711

712 Table 4. Correlation coefficients (R) and significance levels (*p*) of the linear
 713 relationships between CDOM absorption, DOC, salinity and fluorescent components.

714

	a(254)	a(280)	a(350)	DOC	Salinity	C1	C2	C3	C4
DOC	0.711**	0.646**	0.294*	1.000**					
Salinity	0.650**	0.579**	0.159	0.965**	1.000**				
C1	0.850**	0.875**	0.873**	0.496**	0.383**	1.000**			
C2	0.677**	0.686**	0.885**	0.414**	0.270*	0.796**	1.000**		
C3	0.452**	0.417**	0.134	0.648**	0.685**	0.267*	0.103	1.000**	
C4	-0.040	-0.016	0.078	-0.101	0.135	0.084	0.069	0.225	1.000**

715 ***p*< 0.01 level ; **p*<0.05 level.

716

717

718

719

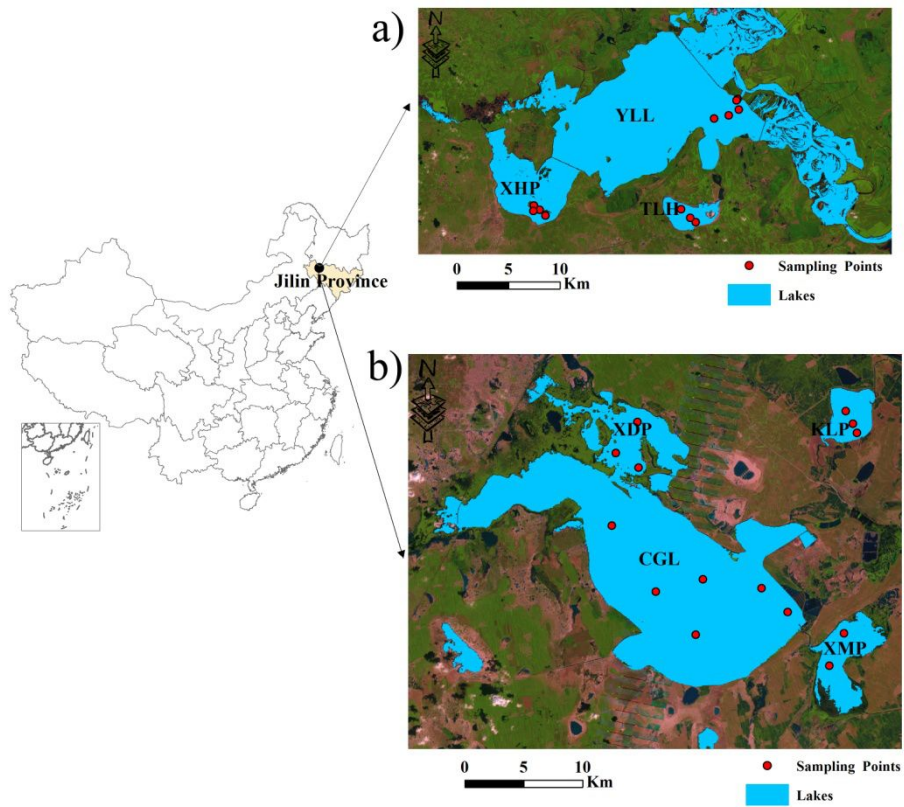
720

721

722

723

724



725

726 Figure 1. Locations of the water sampling sites for 7 lakes in the western part of Jilin
 727 province, Northeast China. a) Yueliang lake group: YLL, Yueliang Lake; XHP;
 728 Xinhuangpao; TLH; Talahong; b) Chagan lake group: CGL, Chagan Lake; XDP,
 729 Xindianpao; XMP, Xinmiaopao; KLP, Kulipao.

730

731

732

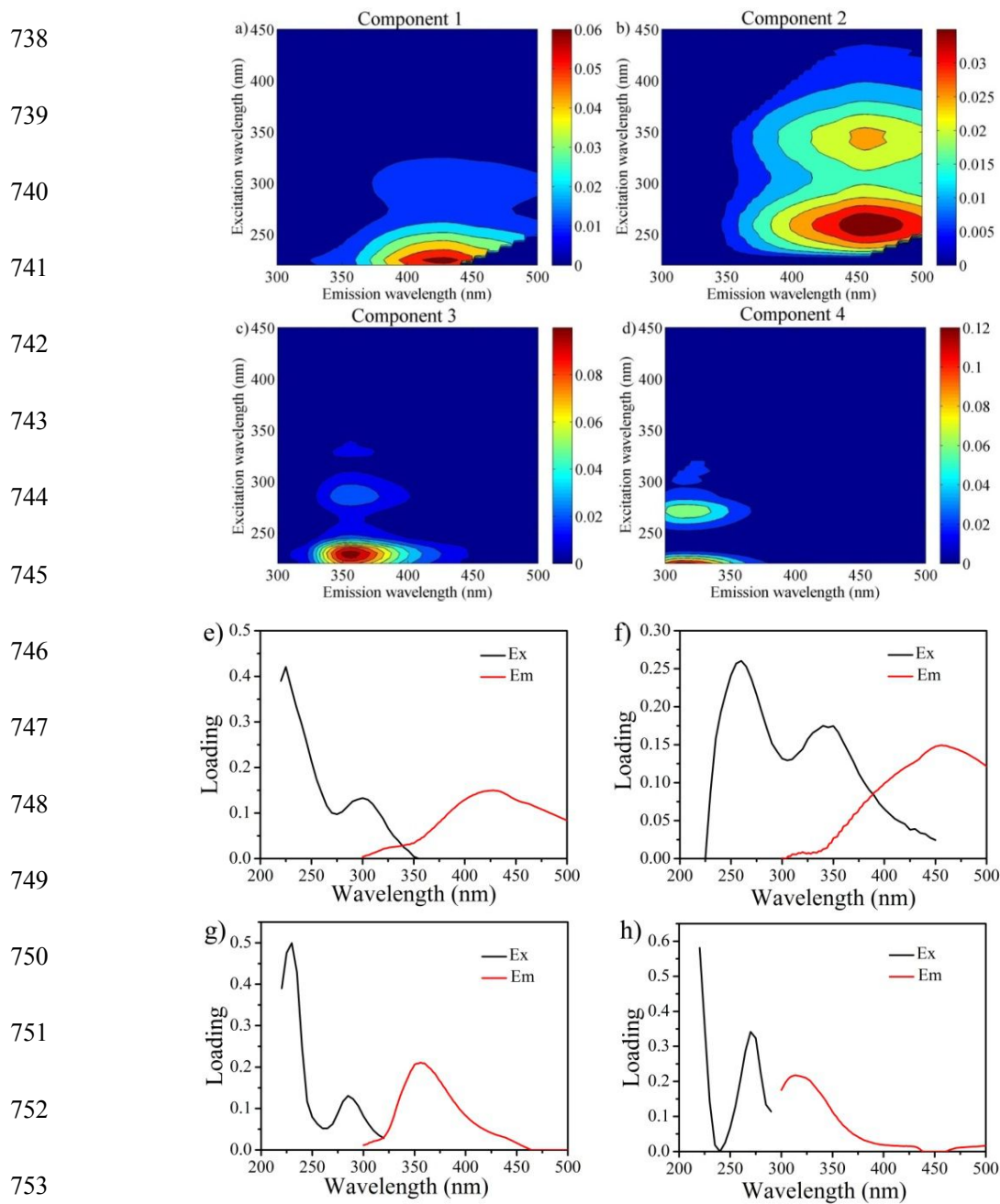
733

734

735

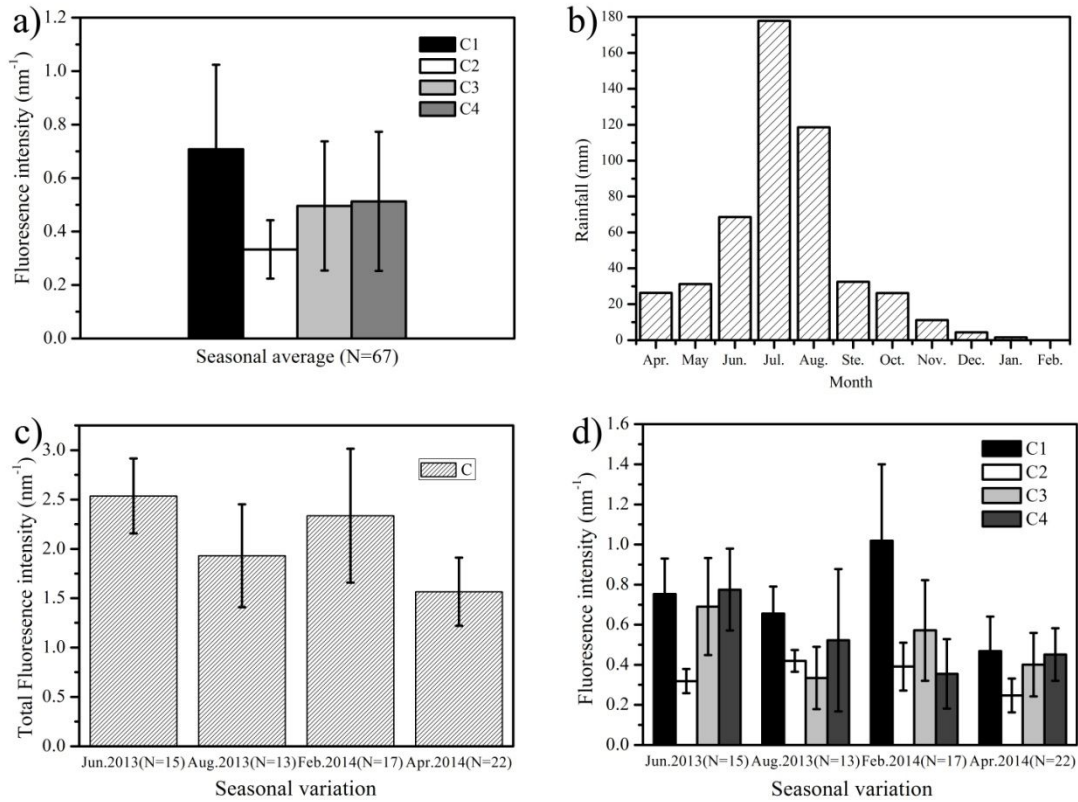
736

737



754 Figure 2. The PARAFAC model output shows the contour plots of the four
 755 PARAFAC fluorescent components (a-d) and excitation (black) and emission (red)
 756 loadings (e-h) of each component. Fluorescence is in Raman units: nm^{-1} .

757



758

759 Figure 3. a) Seasonal average of F_{max} for EEM-PARAFAC components (C1, C2, C3

760 and C4) for lakes in the western part of Jilin province; b) Monthly variation of rainfall

761 for the lakes in western part of Jilin province from April 2013 to February 2014; c)

762 Seasonal variation of the total fluorescence intensity at different seasons; d) Seasonal

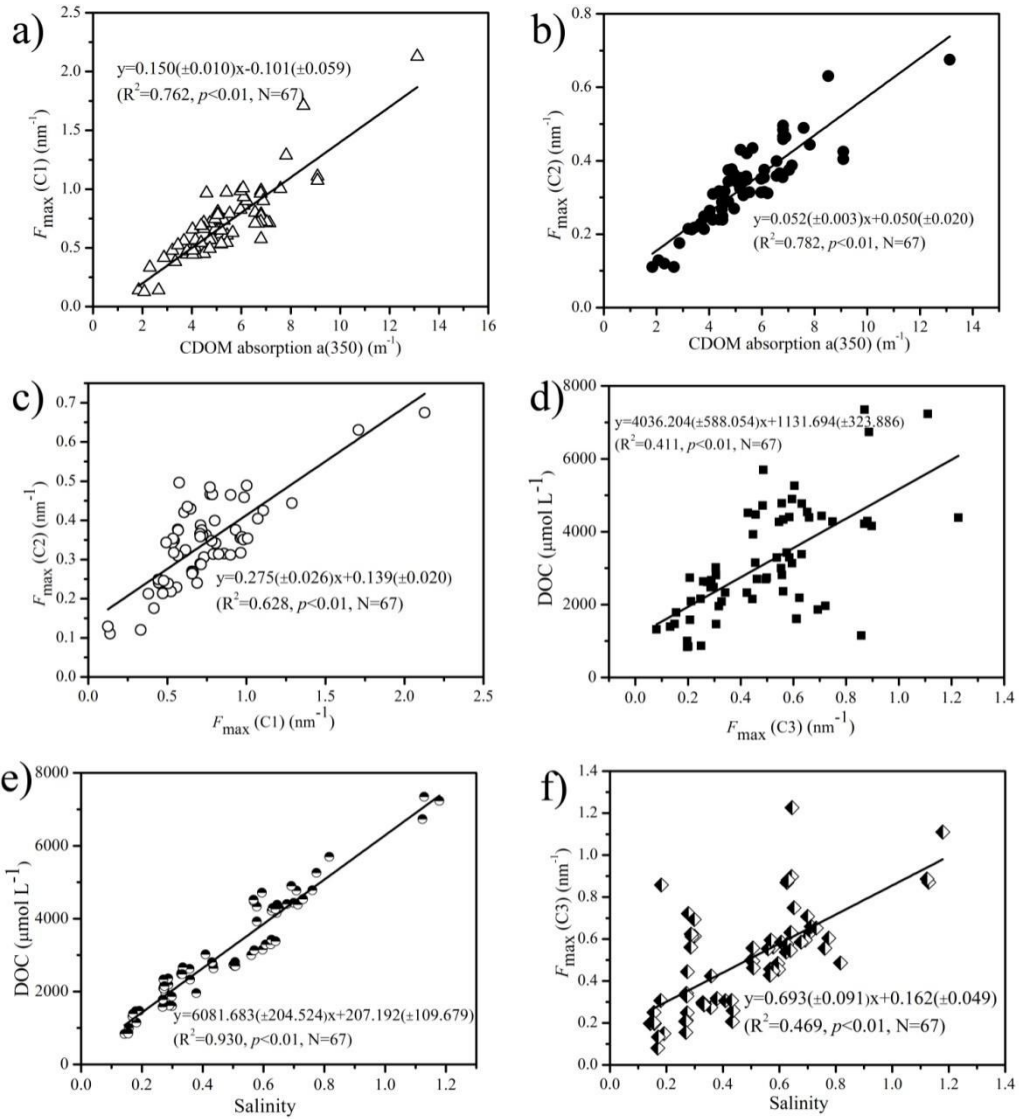
763 variation of the four EEM-PARAFAC components at different seasons. The error bars

764 represent one standard deviation.

765

766

767



768

769 Figure 4. Relationships between CDOM absorption coefficient $a(350)$ with a)

770 $F_{max}(C1)$, b) with $F_{max}(C2)$, c) $F_{max}(C1)$ versus $F_{max}(C2)$, d) $F_{max}(C3)$ versus DOC, e)

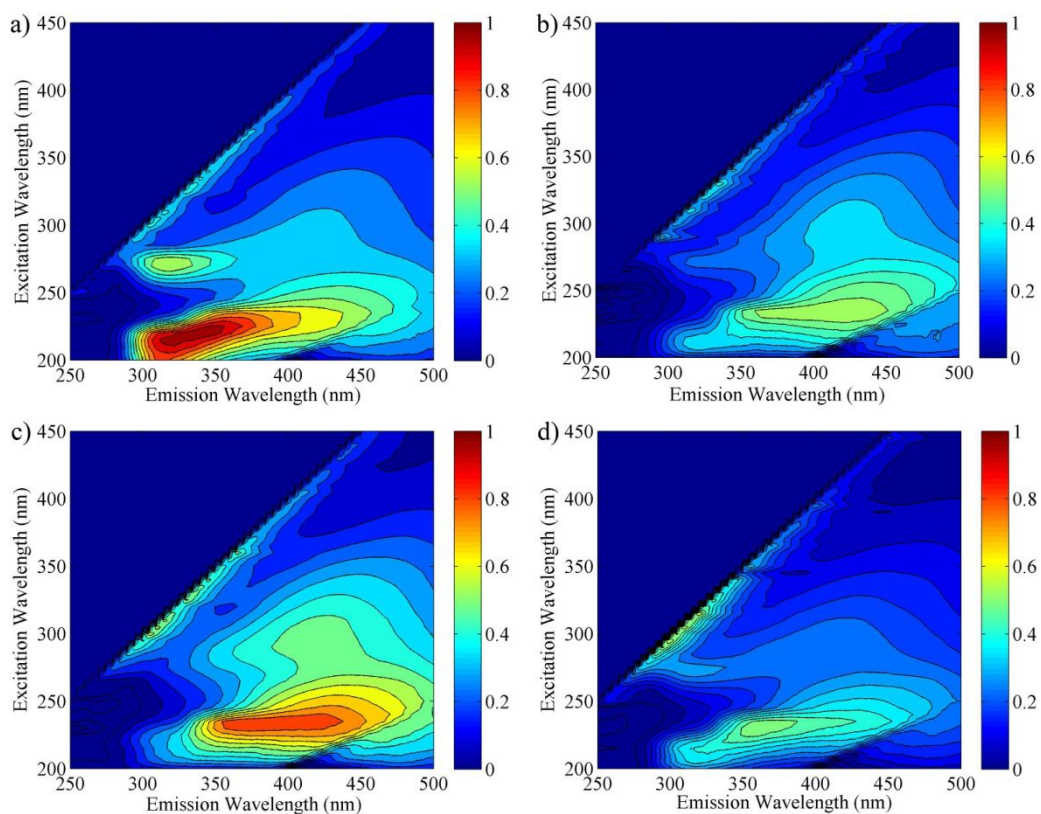
771 Salinity versus DOC, f) Salinity versus $F_{max}(C3)$.

772

773

774

775



776

777 Figure S1. Examples of EEMs for one water sample from Xindianpao Lake in the
 778 western part of Jilin province at different seasons a) June 2013; b) August 2013; c)
 779 February 2014; d) April 2014 (Fluorescence is in Raman unit: nm^{-1}).

780

781

782

783

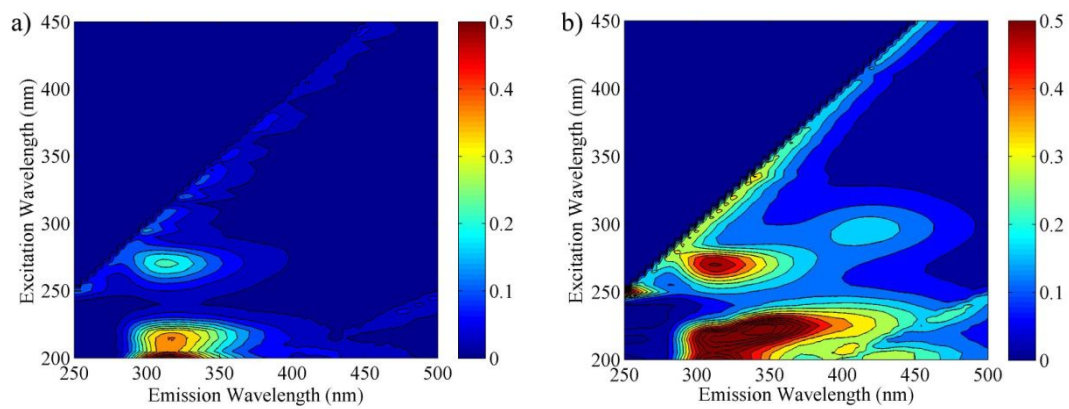
784

785

786

787

788



789

790 Figure S2. Representative examples of EEMs for a) lake ice-melt water sample, and b)

791 rainwater CDOM in the western part of Jilin province (Raman: nm^{-1}).